

Article

# Physical Model Experiments on Water Infiltration and Failure Modes in Multi-Layered Slopes under Heavy Rainfall

Junfeng Tang <sup>1</sup>, Uchimura Taro <sup>1</sup>, Dong Huang <sup>2</sup>, Jiren Xie <sup>3</sup> and Shangning Tao <sup>1,\*</sup>

<sup>1</sup> Department of Civil & Environmental Engineering, Saitama University, Saitama 338-8570, Japan; tanger@imde.ac.cn (J.T.); uchimurataro@mail.saitama-u.ac.jp (U.T.)

<sup>2</sup> Institute of Mountain Hazards and Environment, Chinese Academy of Science, Chengdu 610041, China; dhuang@imde.ac.cn

<sup>3</sup> Department of Civil Engineering, Central South University, Changsha 410012, China; jirenxie198911@csu.edu.cn

\* Correspondence: to.s.670@ms.saitama-u.ac.jp; Tel.: +81-048-858-9002

Received: 30 March 2020; Accepted: 11 May 2020; Published: 17 May 2020



**Featured Application:** Authors are encouraged to provide a concise description of the specific application or a potential application of the work. This section is not mandatory.

**Abstract:** To assess the influence of an intermediate coarse layer on the slope stability during heavy rainfall, knowledge about water movement and how slope failure occurs is important. To clarify the characteristics of water infiltration in a multi-layered slope and assess its influence on the slope failure modes, eight groups of physical slope models were investigated. It was found that the unsaturated hydraulic conductivity in the coarse layer ( $5.54 \times 10^{-6}$  cm/s) was much lower than that of the fine layer ( $1.08 \times 10^{-4}$  cm/s), which resulted in the capillary barrier working at a lower water content. Intermediate coarse layers embedded between finer ones may initially confine the infiltration within the overlying finer layers, delaying the infiltration and eventually inducing a lateral flow diversion in the inclined slope. Two different failure modes occurred in the model experiments: surface sliding occurred at the toe in the single-layer slope group and piping occurred at the toe in the multi-layered slope as the rainfall water accumulated, was diverted along the interface, and then broke through in the downslope direction of the intermediate coarse layer. The lateral flow diversion caused by the capillary barrier and the tilt angle may be the major factors influencing the difference of the failure modes. The result also revealed that the coarser layers may have negative effects on the slope stability.

**Keywords:** unsaturated soil; capillary barrier; multi-layer slope; slope failure

## 1. Introduction

Rainfall-induced slope failure is one of the most destructive natural disasters that occur in shallow natural slopes. The impacts of such catastrophic events are known, but these recurring natural hazards still result in many significant casualties and economic losses [1,2].

This study deals with a slope consisting of a fine layer and an intermediate coarse layer. The presence of soil layers with different unsaturated hydraulic conductivities in a shallow depth of soil affects the process of water infiltration, distribution, and pore water pressure in the slope, which results in different failure modes [3]. Rainfall infiltration water is due to the build-up of capillary barriers [4], which accumulate at the interface between fine and coarser soil layers. The capillary barrier effect has been widely studied in terms of its use in cover systems in waste disposal sites [5,6], whilst more recent research has focused on slope stabilization [7].

Capillary barriers can maintain a high degree of saturation in the soil above them, which results in different failure parts in a multi-layer slope [8]. These phenomena are related to the capillary tension, which limits the downward movement of the wetting front from a finer soil into underlying coarser soil. In an inclined interface, under continuous water infiltration from the slope surface, the accumulated water above the interface between the fine and the coarse material leads to the formation of a gravity-driven sub-surface water flow along the interface. This depends on the geometrical or boundary variations, at a certain distance downslope, often reported as the “diversion length”, which can be estimated using a model proposed by Ross [9]. In natural slopes, characterized by a length in the order of hundreds of meters and an irregular layer geometry, the conditions leading to the penetration of infiltrating water into the underlying coarse layer are mainly governed by the materials, slope angle, and infiltration rate [10].

In some field investigations, a multi-layered slope with different hydraulic conductivities is a common situation in layered hillside slopes. Such a slope consists of fine sand deposits and medium-coarse sand deposits that are a few meters thick [11]. Additionally, the inclined angles range from 10 to 35 degrees. The coarse sand deposits involved have been found to have large pores and a higher hydraulic conductivity in a saturated condition, which have an important influence on the subsurface water flow and water content distribution during the infiltration, steady percolation, and drainage [12,13]. A schematic of a three-layer distribution in a slope is presented in Figure 1.

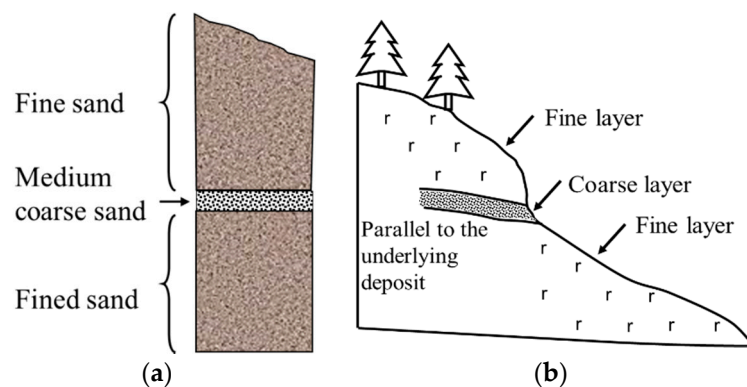


**Figure 1.** (a) Schematic profile of a multi-layered slope; (b) a description of the geometry of a multi-layered slope.

Many previous field investigations have been conducted and have found that layered soil influences the process of rainfall water movement and the distribution of water content, which determines the slope failure. However, clarifying the influence of an intermediate coarse layer on slope failure is still a complex issue, since many uncontrollable factors exist in a natural slope, such as the slope angle, rainfall intensity, etc. Hence, slope model experiments replacing field monitoring have been conducted, as these allow the same slope in different conditions to be investigated, reduce the cost by reducing the duration, and consider variable slope types [14].

To investigate the infiltration process in a layered soil profile in simplified and known geometrical and boundary conditions, physical model experiments have been performed by many researchers. Infiltration experiments have been conducted and have indicated that the wetting front temporarily stops above the interface of the fine layer and coarse layer, and the infiltration rate slows down [15,16]. Additionally, the pore water pressure head of the finer layer above the soil interface could not increase when the water started to infiltrate into the coarse layer [17]. The presence of a coarser lower-most layer may confine the infiltration within the upper finer layer up to a high degree of saturation. This capillary barrier effect occurred in a slope and was considered to be the cause of landslide initiation [7]. A capillary barrier at the upper interface of a coarse layer could have developed, favoring the accumulation and a lateral distribution of infiltrating rainfall and a possible diversion of flow down the slope, thus leading to a localized increase in the water content and loss of strength [18].

A diversion of the flow from the vertical direction towards the slope direction occurs and part of the water crosses the coarse layer infiltrate into the deepest layer. The settlement of soil is accompanied by progressive saturation of the soil, but general slope failure does not take place in the whole process [19].

Although some model experiments have been conducted to analyze the water movements and post-failure evolution due to the capillary barrier effect, few model experiments have focused on the slope failure time and modes in single- and multi-layer slope conditions or analyzed how an intermediate coarser layer may affect the slope stability.

Therefore, the aims of this study were as follows: (1) to experimentally clarify the influence of intermediate layers on water movement in a horizontal and inclined slope, respectively, especially after the breakthrough of the capillary barrier and (2) to investigate its influence on slope failure modes and the failure time in a single-layer and multi-layer slope by monitoring the water content, pore water pressure, and failure modes at different tilt angles. Soil-water characteristic curves (SWCC) [20] of fine sand and coarse sand were also measured to explain how the capillary barrier works. The proposed physical model experiments can provide a perspective on the failure time and modes of a single- or multi-layered slope during a rainfall event.

## 2. Materials and Methods

### 2.1. Basic Material Properties

Silica sands S1 and S7 were chosen for the physical model experiments as the fine material and coarse material, respectively, by the difference of  $D_{50}$  and size distribution. Figure 2 shows the size distribution of S1 (fine material) and S7 (coarse material) used in model experiment. Table 1 summarizes the specific properties of S1 and S7 used in the model experiments. The sieve tests were conducted using the JGS Geotechnical Society standard test methods (JGS0131-2009).

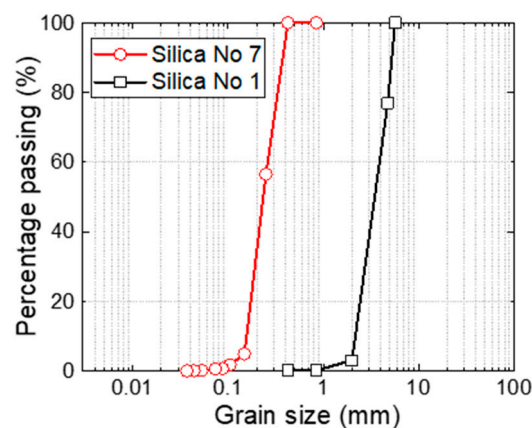


Figure 2. Grain size distribution of S1 and S7 in physical model experiments.

Table 1. Basic properties of sand materials.

Description	Silica No 7	Silica No 1
Specific gravity $G_s$	2.63	2.62
Gravel content (>4.75 mm; %)	0	97.13
Sand content (%)	87.31	2.86
Fines content (<0.075 mm; %)	11.64	0
$D_{10}$ (mm)	0.043	2.26
$D_{50}$ (mm)	0.152	3.52
$D_{60}$ (mm)	0.165	4.21
Maximum dry density ( $\text{g}/\text{cm}^3$ )	1.556	1.52
Minimum dry density ( $\text{g}/\text{cm}^3$ )	1.271	1.3

The unsaturated hydraulic properties were measured by the variable head method (ASTM 2006) D2434-68. Table 2 and Figure 3a show the fitting parameters of the VG (van Genuchten–Mualem) model [21] and soil-water characteristic curves of silica No 1 and 7 in both the drying process and wetting process. The unsaturated hydraulic conductivities of sands were obtained by a pressure plate apparatus in the lab. As shown in Figure 3a, the drying (desorption) process and the wetting (absorption) process of the SWCCs of sand cause hysteretic behavior [15] for the same suction value, and the sand can retain more water in the drying process than in the wetting process. In the wetting process, the air entry value (AEV) of the fine layer (silica No 7) is about 1.5 kPa. The AEV of sand and gravel is about 0.45 kPa, being lower than the AEV of the fine layer. The capillary barrier effect occurs at the fine-coarse sand interface during rainfall infiltration. In Figure 3b, the unsaturated hydraulic conductivities of two types of sand are reported. The obtained values range between  $10^{-2}$  and  $10^{-7}$  cm/s under different suction conditions. The results show that the hydraulic conductivity of the coarse sand is higher than that of the fine sand at almost saturation, while it is significantly lower when the soil is unsaturated.

The soil-water characteristic curves of the soil were modeled with the van Genuchten–Mualem model [5], as follows:

$$S_e = \{1 + (-ah)^n\}^{-m}, S_e = \frac{\theta - \theta_r}{\theta_s - \theta_r}, m = 1 - \frac{1}{n}. \tag{1}$$

In the above equation, the water retention curve is expressed in terms of the effective degree of saturation.  $\theta$  is the volumetric water content;  $\theta_r$  and  $\theta_s$  indicate the residual and saturated values of the water content, respectively;  $a$ ,  $m$ , and  $n$  are the fitting parameters;  $h$  is the matric suction;  $a$  is a scaling parameter (units of  $m^{-1}$ ); and the exponents  $n$  and  $m$  are parameters that determine the shape of the retention curve. The hydraulic parameters are given in Table 2.

**Table 2.** Hydraulic properties of sand materials.

Description	Symbol (unit)	Soil	
		No 7	No 1
Drying curve			
Saturated volume water content	$\theta_s$	0.44	0.42
Air-entry value	$\psi_a$ (kPa)	2.44	0.62
Residual volume water content	$\theta_r$	0.12	0.05
van Genuchten model	$a$	0.41	1.59
Fitting parameter	$n$	4.07	3.11
Fitting parameter	$m$	1.42	0.67
Wetting curve			
van Genuchten model	$a$	0.42	0.03
Fitting parameter	$n$	4.51	1.42
Fitting parameter	$m$	0.78	0.29

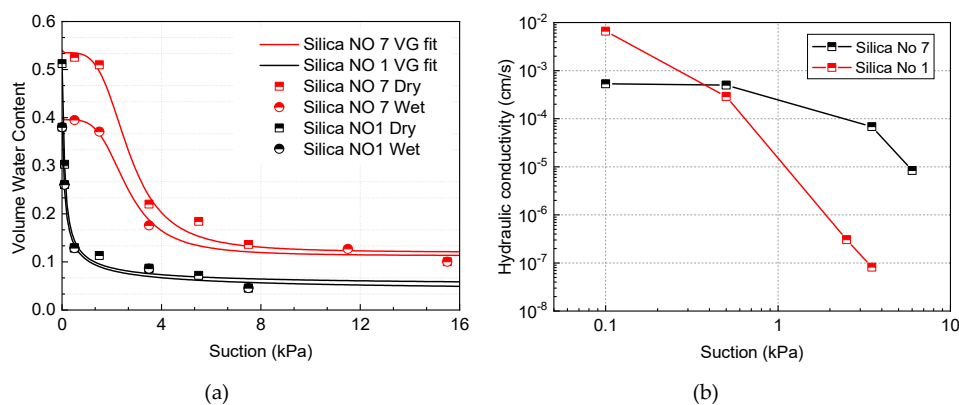


**Figure 3.** (a) Soil-water characteristic curves (SWCCs) of silica No 1 and No 7 in the drying and wetting process; (b) unsaturated hydraulic conductivity of silica No 1 and No 7 in the wetting process.

### 2.2. Water Flow and Slope Failure in Multi-Layer Slope Models

The multi-layer models were set up to evaluate the effect of the capillary barrier acting on a slope. This model system was built to show the advancement of the wetting front, and monitor the volumetric water content in the soil, pore water pressure, and slope failure process. In addition, the failure process was directly recorded by cameras to obtain a better understanding of failure modes and the effect of the capillary barrier. Table 3 summarizes the physical experimental conditions.

**Table 3.** General information for the slope model experiment.

Experiment	Sediment Type	No. of Layers	Tilt Angle (°)	Rainfall Intensity	Depth of Layers
Case I	S1, S7	3	0	75 mm/h	0.2 m, 0.05 m, 0.2 m
Case II	S1, S7	3	7	75 mm/h	0.2 m, 0.05 m, 0.2 m
Case III	S1, S7	3	15	75 mm/h	0.2 m, 0.05 m, 0.2 m
Case IV	S1, S7	3	21	75 mm/h	0.2 m, 0.05 m, 0.2 m
Case V	S7	1	0	75 mm/h	0.45 m
Case VI	S7	1	7	75 mm/h	0.45 m
Case VII	S7	1	15	75 mm/h	0.45 m
Case VIII	S7	1	21	75 mm/h	0.45 m

#### 2.2.1. Flume Model System

Figure 4a shows the apparatus used for the physical model experiments, which consisted of an inclined steel box, a rainfall simulation system, and a set of pore water pressure and VWC (volumetric water content) sensors. The details of each subsystem are as follows: (i) the inclined steel box had dimensions of 1.0 m (length) × 0.3 m (width) × 0.5 m (height); (ii) the sidewalls of the box were made of an acrylic plate to observe the advancement of the wetting front and failure process during rainfall. The gap between the steel plates and the acrylic plate was sealed with epoxy adhesive.

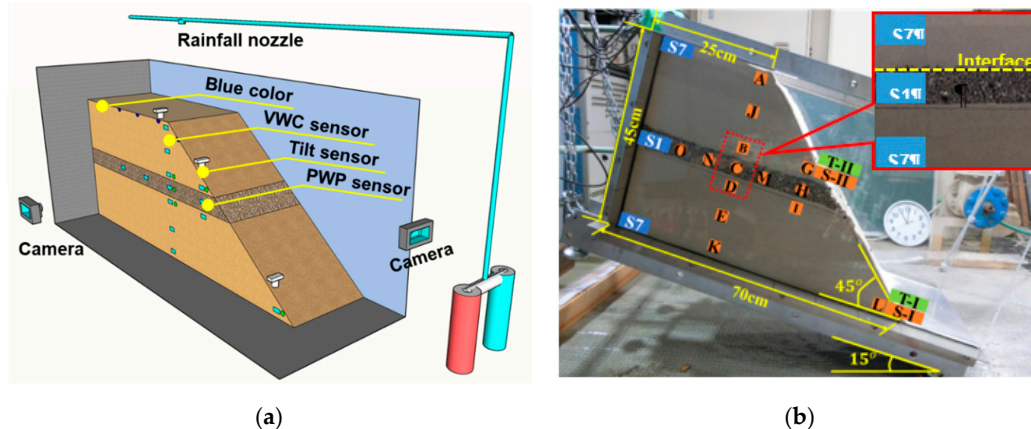


**Figure 4.** (a) Schematic diagram of the experimental apparatus used for a multi-layered slope under rainfall: side-view of the multi-layered slope; (b) side view of the experimental apparatus used for the slope. The yellow dashed line shows the fine–coarse interface.

Furthermore, the inclined angle of the model box could be lifted by a crane to simulate the inclined cover from 0 to 60 degrees. Experiment pictures were recorded by cameras in different locations around the model. Table 3 summarizes the physical model experimental conditions.

#### 2.2.2. Rainfall Simulation System

A rainfall nozzle was placed 60 cm above the model box to simulate rainfall with a constant intensity. The intensity and duration of rainfall were controlled by a control valve and air pressure gauge. The rainfall intensity was kept at a constant intensity by air pressure, and ranged from 35 to 100 mm/h. The sensors ECH2O EC-5 were used to determine the volumetric water content. Soil-specific

calibration is recommended for obtaining the best possible accuracy in volumetric water content measurements [22,23]. Calibration of the EC-5 sensors has been shown to result in an increased accuracy of 1–2% for all soils with soil-specific calibration [24,25]. The calibration of EC-5 sensors employed in silica No 1 and No 7 is shown in Figure 5b.

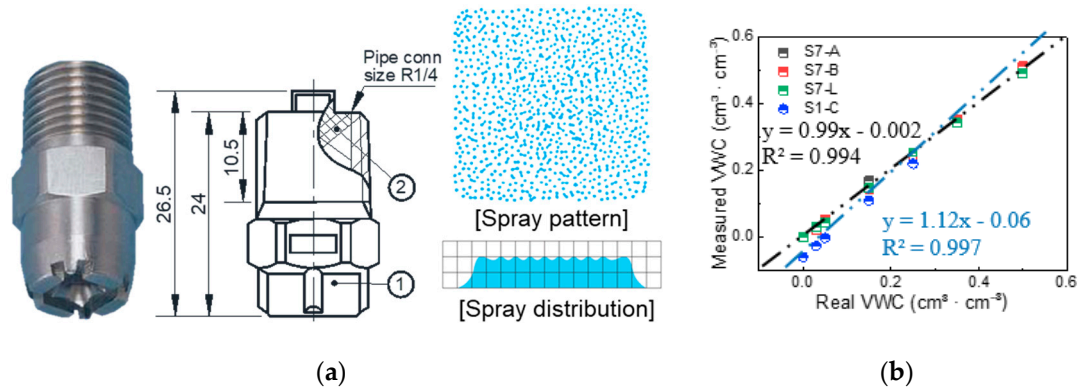


**Figure 5.** (a) Nozzle body and spray pattern and distribution for rainfall simulation; (b) calibration of the volumetric water content sensor in silica No 1 and No 7.

### 2.2.3. Theory of Measurement Devices

The instruments used in the model experiments were calibrated before installation, including the pore water pressure, tilt sensors (Figure 6a), VWC sensors (Figure 5b), and rainfall simulators (Figure 5a). The intensity and uniformity of artificial rainfall created by the simulator were calculated based on the weight of the sample at a certain time.

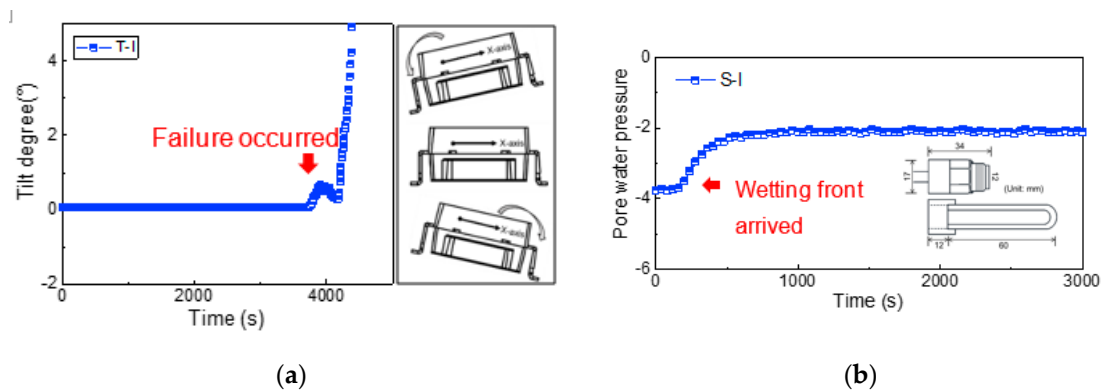


**Figure 6.** (a) MEMS (Micro-Electro-Mechanical System) tilt sensor and its working theory; (b) typical pore water pressure response in soil and the structure and size of the transducer.

### 2.2.4. Testing Procedure

#### Soil Preparation

S1 and S7, which were used to make the slope, were dried in an oven for 48 h. Then, an amount of water was added to the soil to achieve an initial water content of around 6%.

#### Compaction of Soils

The prepared soil was compacted and placed in a series of horizontal layers. Silica No 7 and No 1 were placed in the model box in layers and compacted to achieve a dry density of 1.33 and 1.43 g/cm<sup>3</sup>, respectively. Each layer was tamped equally with a rod to a thickness of 5 cm and these procedures were repeated until the height of the slope was achieved.

### Positions of Sensors and Cameras

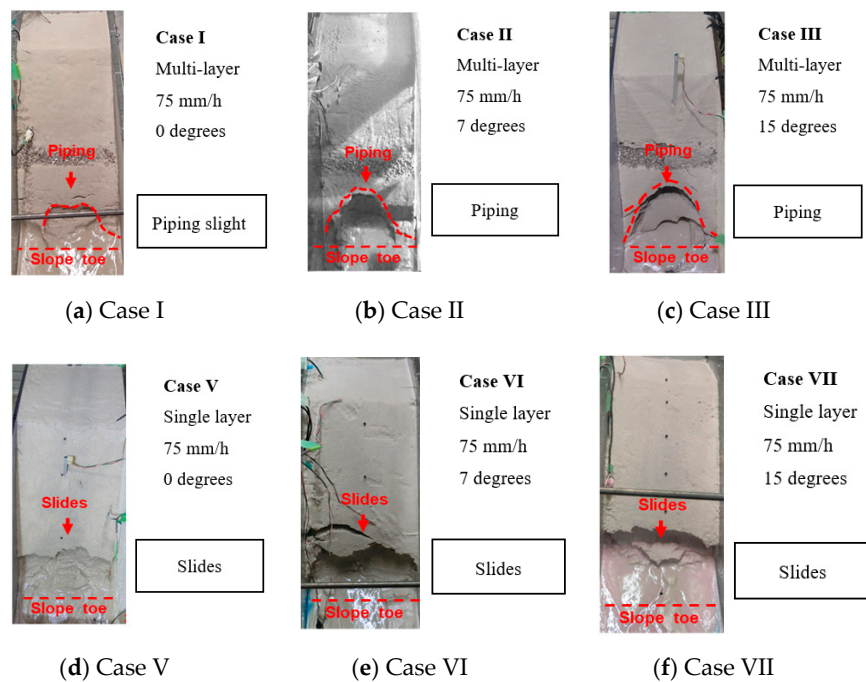
During the soil placement, VWC sensors, tensiometers, and tilt sensors were placed at specific locations in the three different layers and the time of recording the quantity of water content was 10 s.

Table 3 summarizes all of the experimental conditions.

## 3. Results

### 3.1. Failure Situations in All Cases

Figure 7 shows the failure situations for different cases during rainfall. No runoff on the surface of the slope was observed in all cases, as the infiltration capacity of the soil layer was higher than the rainfall intensities used in this study. Two failure modes were observed in this study. One was soil piping, which occurred in the multi-layered slope. Slight soil piping occurred at the toe of the slope, finer materials mixed with amounts of infiltrate water flowed out from the piping as the seepage surface, and the seepage surface grew gradually and increased until cracks appeared (Figure 7c). As Figure 7a shows, the piping phenomenon occurred slightly, and as the tilt angle increased, the soil pipe size developed rapidly and more seriously (see Figure 7b,c).



**Figure 7.** Comparison of failure situations of the different model experiment cases (each case was performed three times to ensure the repeatability of the results, and typical results of individual experiments were chosen to show the failure situation in each case). (a) case I (tilt angle  $\alpha = 0^\circ$ ); (b) case II (tilt angle  $\alpha = 7^\circ$ ); (c) case III (tilt angle  $\alpha = 15^\circ$ ); (d) case V (tilt angle  $\alpha = 0^\circ$ ); (e) case VI (tilt angle  $\alpha = 7^\circ$ ); (f) case VII (tilt angle  $\alpha = 15^\circ$ ).

Another failure mode was surface sliding from the toe of the slope in a single-layer slope. Small slide failure occurred at the toe at first, and then relatively larger slide failure followed. This type of failure mode was clearly observed for cases IV, V, and VI, as shown in Figure 7d.

The failure modes and initial failure time  $t$  for all eight cases are summarized in Table 4. The initial slope failure occurred at the toe of the slope in case I and case IV at about 1.18 and 0.95 h after the rainfall has been applied, respectively. This means that failure in a multi-layer slope occurs later than that in a single layer under the same condition in the horizontal group. In Figure 7b,e, in case II and case V, failure occurred at around 0.84 and 0.89 h, respectively. In case III and case VI, more rapid

movement of slope failure occurred in an almost fully saturated condition and they thus had a lower strength. The failure times of the 15 degrees inclined group were 0.78 and 0.85 h. It should be noted that failure occurred earlier in the multi-layer slope than in the single-layer slope in the inclined group, which is different from the result obtained for the horizontal group.

**Table 4.** Failure conditions of physical model experiments.

Experiment	Rainfall Intensity $I$	Tilt Angle $\alpha$ ( $^{\circ}$ )	Failure Modes	Initial Failure Time $t$ (h)
Case I	75 mm/h	0	Piping slightly	1.18 h
Case II	75 mm/h	7	Piping	0.84 h
Case III	75 mm/h	15	Piping	0.78 h
Case IV	75 mm/h	21	Piping	0.62 h
Case V	75 mm/h	0	Surface slides	0.95 h
Case VI	75 mm/h	7	Surface slides	0.89 h
Case VII	75 mm/h	15	Surface slides	0.85 h
Case VIII	75 mm/h	21	Surface slides	0.76 h

### 3.2. Profile of the Volumetric Water Content in a Slope

During the tests, the hydrological response was monitored by means of VWC (volumetric water content) sensors located at different locations within the slope and crossing the entire soil thickness, allowing the retrieval of volumetric water content profiles at different depths. The VWC sensors in section I in different cases were shown to explain how the capillary barrier effects influence the water infiltration and distribution during the rainfall and drying process, as is shown in Figure 8 (the sensor locations are shown in Figure 4b). Throughout the experiment, the VWC of the toe of slopes increased slowly with time toward a saturated value in response to the saturation process, until failures occurred. It should be noted that the capillary barrier clearly controlled the rate of changes of the VWC in a multi-layer slope, which determined the failure time of slope.

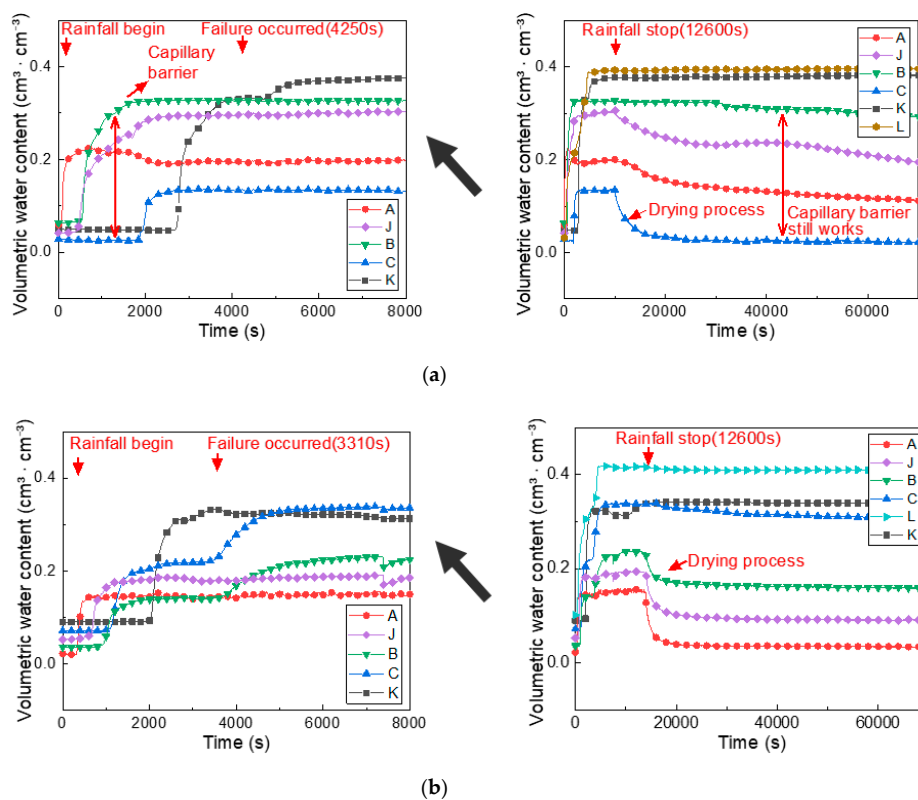


**Figure 8.** Cont.

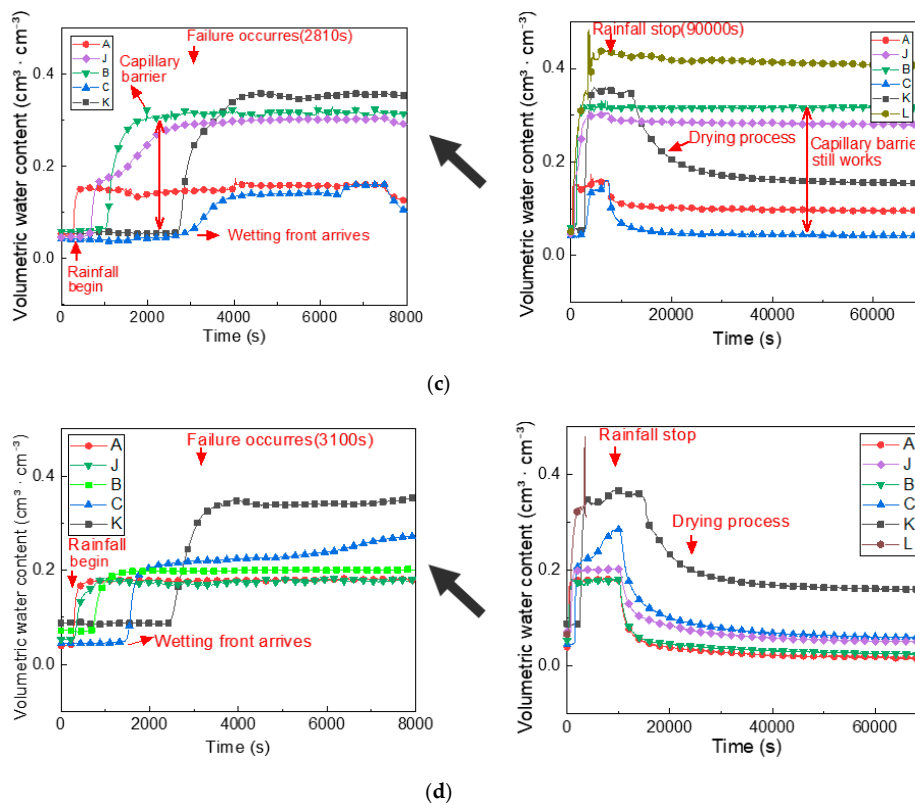


**Figure 8.** Time histories of VWC during rainfall and the drying process in case I, III, V, and VII (the left figures show the time from 0 to 8000 s, while the right figures show the whole wetting and dry process in the rainfall event). (a) Case I. VWC trends in a multi-layer slope in the flat group (tilt angle  $\alpha = 0^\circ$ ); (b) Case V. VWC trends in a single-layer slope in the flat group (tilt angle  $\alpha = 0^\circ$ ); (c) Case III. VWC trends in a multi-layer slope in the inclined group (tilt angle  $\alpha = 15^\circ$ ); (d) Case VII. VWC trends in a multi-layer slope in the inclined group (tilt angle  $\alpha = 15^\circ$ ).

In case I and case V (see Figure 8a,b), the advancement of the wetting front is evident from the time history of the VWC sensors. It shows that the rise of the VWC was rapid, and then became gradual, as the toe of the slope approached a fully saturated condition. When the VWC at point L reached around 0.4, failure occurred at the toe of the slope. In addition, compared with the VWC at point L in the flat group, point L reached the saturated condition later in the multi-layer model, since the capillary barrier prevented the water from infiltrating into the bottom. This made the slope more stable and caused a delay in the failure time, which was 1.2 and 0.92 h in case I and case III, respectively. This capillary barrier effect can also be explained by the VWC histories obtained during the experiments. For example, it took around 26 min for the wetting front to pass through the interface from point B to point C [11].

Figure 8c,d show that when rainfall was applied, the VWC increased quickly above the interface (point B), and when rainfall was stopped, the soil above the coarse layer (point B) remained wetter than the same location in a single-layer slope. Additionally, for the VWC at the toe of the slope (point L) in the inclined group, the failure occurred earlier (0.78 h), while it was 0.84 h in a single-layer slope, which was contrary to the flat group experimental results.

### 3.2.1. Beginning of Rainfall ( $t = 0$ h)

In case I and V, the VWC in the bottom of the upper fine layer (point B) increased from 0.05 to 0.33 with the depth in the upper fine layers (height was from 25 to 45 cm), while that in the coarse layer was about 0.03 before capillary barrier breakthrough at the beginning of rainfall in case I ( $t = 0.5$  h).

This indicates that the wetting front above the interface was stopped for a while and rainfall water was stored in the upper fine layer due to the influence of the capillary barrier. In the lower section I (height was from 0 to 20 cm), the VWC maintained a constant condition while the capillary barrier was present.

### 3.2.2. The Breakthrough of the Capillary Barrier (Case I, II, and III)

During the first 0.8 h of rainfall, as shown in case I and case II in Figure 9 a,b, the presence of the intermediate coarse layer caused a significant time delay in the infiltration process: the VWC in section I above the interface increased to 0.34 in case I, whereas the VWC in the coarse layer changed from 0.03 to 0.05 in case I at the depth of 22 cm, while the VWC was from 0.04 to 0.22 at the same depth in case II ( $t = 0.6$  h). In this stage, the interface between the fine and coarse layer acted as a capillary barrier and gradually broke when the bottom of the upper fine layer was almost at saturation. In case II, the VWC in section I above the interface increased from 0.06 to 0.32, while that of the coarse layer was from 0.03 to 0.04. A lateral diversion flow may have occurred along the inclined interface, resulting in capillary barrier breakthrough occurring later in section I compared with case I.

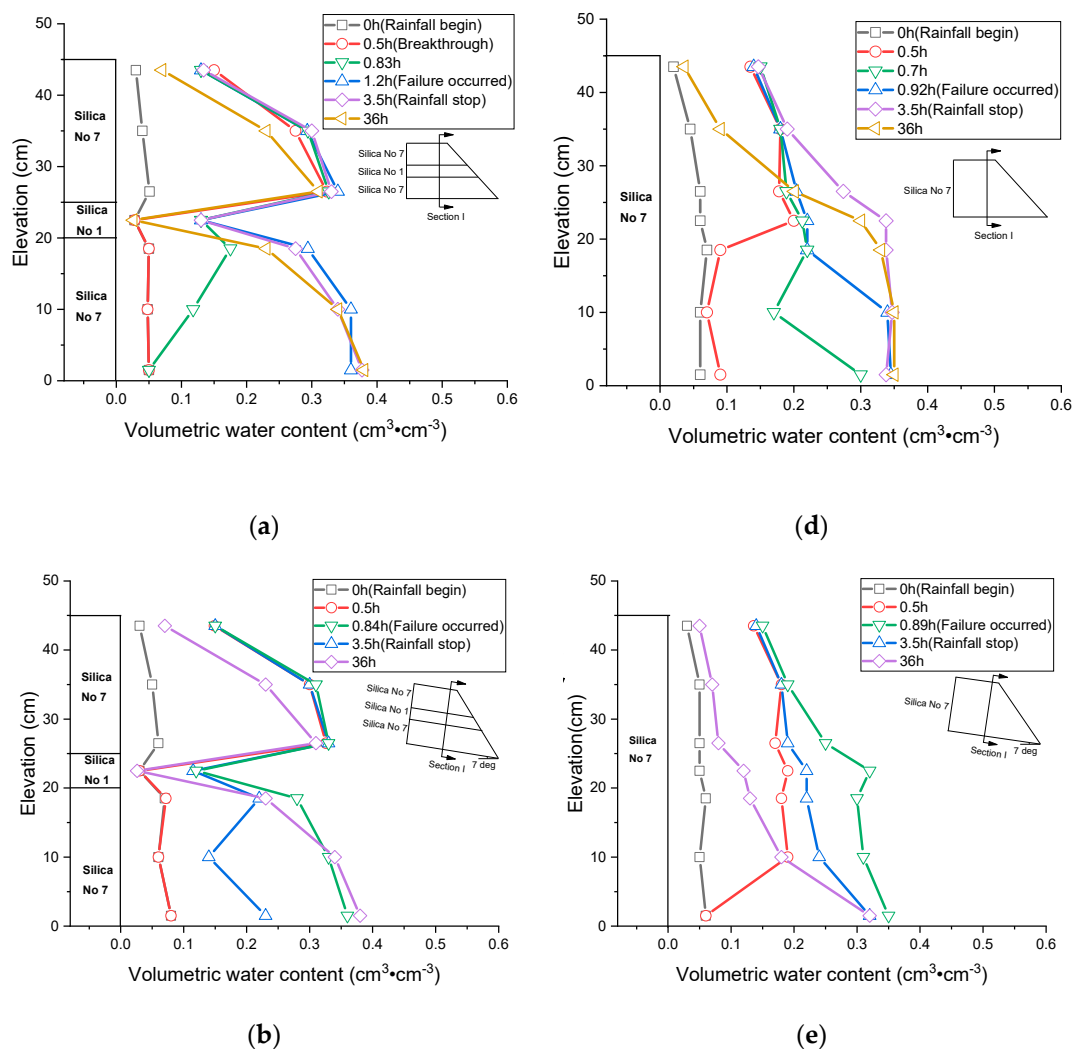
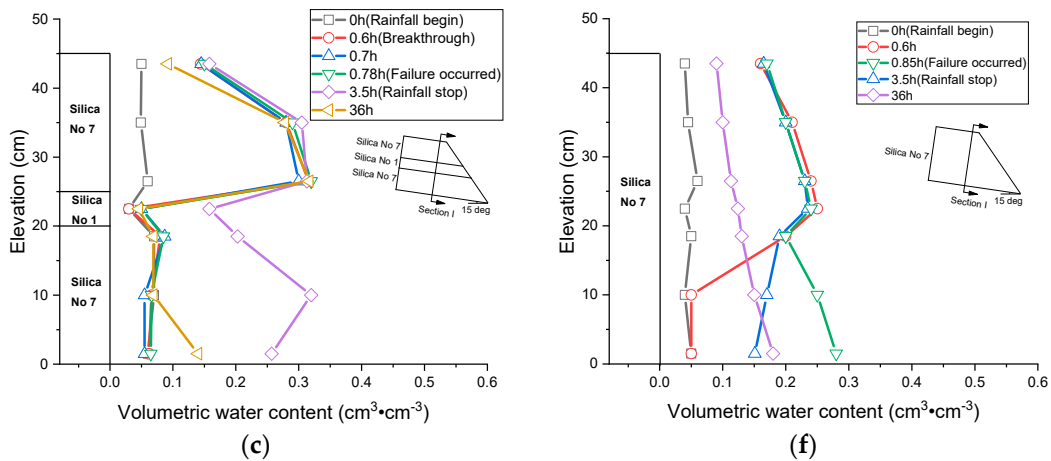


Figure 9. Cont.



**Figure 9.** Profile of the VWC in section I in different cases (the VWC distribution after slope failure was verified by obtaining soil samples from various locations at the end of the experiments). (a) Case I; (b) Case II; (c) Case III; (d) Case V; (e) Case VI; (f) Case VII.

### 3.2.3. Post-Breakthrough of the Capillary Barrier ( $t = 0.6\text{--}0.78$ h in Case I, II, and III)

After 0.6 h of rainfall, the VWC of the upper fine layer maintained a constant value in section I in case I and III, since it reached steady state infiltration in the soil. Additionally, rainfall water infiltrates into the next layer following capillary barrier breakthrough. For example, the VWC of the coarse slayer increased from 0.05 to 0.12 at 0.83 h and 0.13 at 1.2 h (see Figure 9a) in case I and the VWC of the coarse layer increased from 0.05 to 0.07 at 0.78 h in case III. It should be noted that the VWC of the bottom of the lower finer layer increased to 0.36 at 0.8 h in case I and to 0.08 at 0.78 h in case III, respectively. This means that rainfall water could not arrive at the lower fine layer along section I because of the lateral water flow along the inclined interface in case III.

### 3.2.4. Failure Occurred ( $t = 0.78\text{--}1.2$ h)

In this part, the failure process is analyzed using the response of the tilt angle, pore water pressure, and VWC measurements in different locations in the slope. In case III and VII, the experimental flume was tilted to  $15^\circ$  and subjected to the same rainfall intensity. This section aims to evaluate the effects of an inclined angle on the water movement and slope stability.

The main results of this part are reported in Figures 10 and 11. The initial pore water pressure values were negative at the locations of S-I and S-II. The pore water pressure and VWC increased during the infiltration and then stabilized when the infiltration reached a steady state condition. During the rainfall, the tilt angle of point G and point A almost maintained a constant value, while the soil in these locations maintained a negative value. A sudden change occurred when the pore water pressure approached 0 kPa at point L in all cases.

Comparing the difference of the pore water pressure measured at S-II in case I and case V, presented in Figure 10a,b), the pressure grew from  $-4$  kPa at the beginning of the rainfall to around  $-1$  kPa after around 1.2 h above the coarse interface, while it reached  $-3.5$  kPa in case V. This suggests that there was a higher water content and pressure head above the coarse layer than at the same location in a single-layer slope, as the capillary barrier effect led to the storage of water and high water pressure head. In this respect, it is worth noticing that in case I, the pore water pressure at point L (S-I) increased suddenly after capillary barrier breakthrough at the interface.

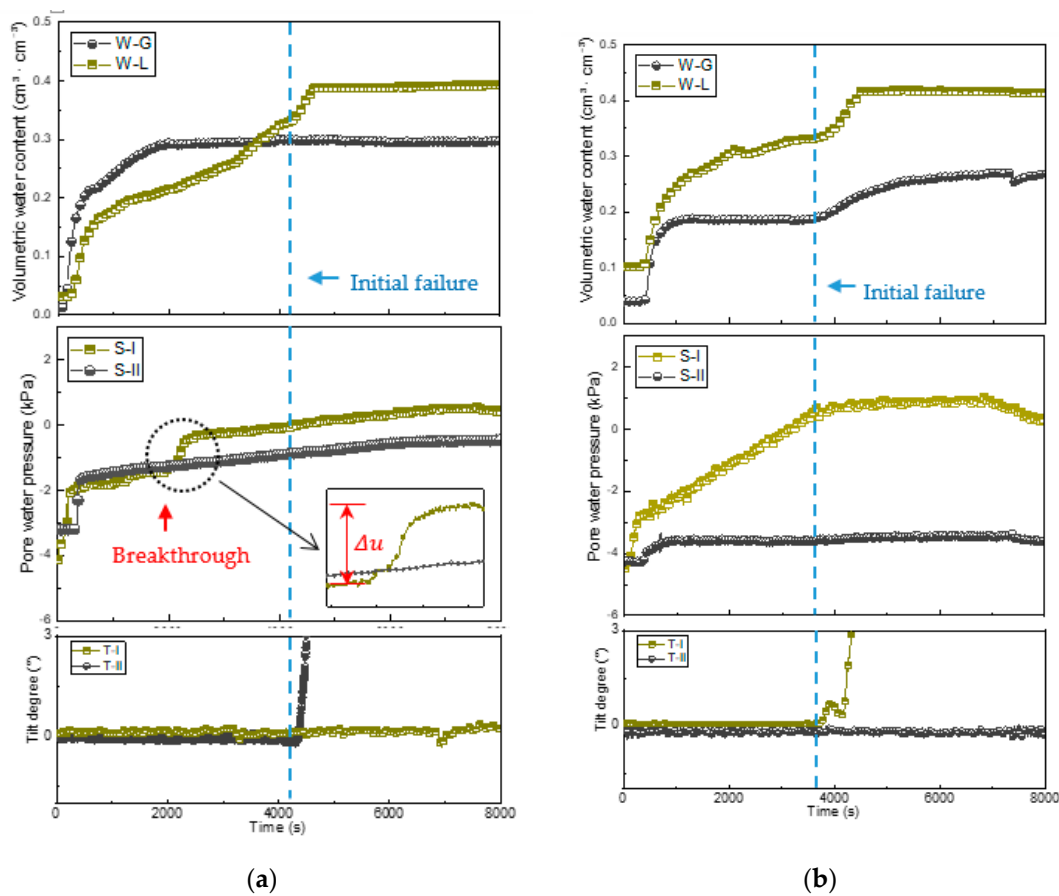


**Figure 10.** Volumetric water content, pore water pressure, and tilt angle change trends at different locations during infiltration. (a) case I (tilt angle  $\alpha = 0^\circ$ , multi-layer), where the pore water pressure increased after capillary barrier breakthrough; (b) case V (tilt angle  $\alpha = 0^\circ$ , single layer). For the positions of sensors, see Figure 3b.

The same behavior, in terms of the pore water pressure and VWC, was observed in tests with the tilt angle  $\alpha = 15^\circ$  (Figure 11). In these two cases, the greater slope angle induced the most sudden variations of water content and pore water pressure, and also resulted in an earlier response of tilt sensors located at the toe of the slope. For case III with the tilt angle  $\alpha = 15^\circ$ , failure occurred in about 0.78 h, and the increase of VWC was more rapid than that of case VII, which was contrary to case VII. In the inclined group, the later failure occurred at 0.84 h in a single-layer slope, which proved that an inclined multi-layer slope is more dangerous than a single-layer one under this condition, which is contrary to the findings of the flat group.

It is evident in Figures 10a and 11a that the increase of the pore water pressure can be divided into two periods. A negative pore pressure was measured at the beginning of rainfall (S-I), and then, around 30 min later, a sudden increase of the pore water pressure value  $\Delta u$  could be measured after capillary barrier breakthrough at point L (Figure 3b). Moreover, a few minutes after breakthrough, piping occurred for a pore pressure of 0 kPa at the toe, which seems to indicate a negative influence for the slope instability. Similar to case I, pore pressure sensor S-I in case III also showed the same trends after the breakthrough of the capillary barrier. It is clear from both data sets that the pore water pressure value increased from  $-1.5$  to  $-0.3$  kPa in case I and from  $-1.1$  to  $-0.21$  kPa in case III, respectively.

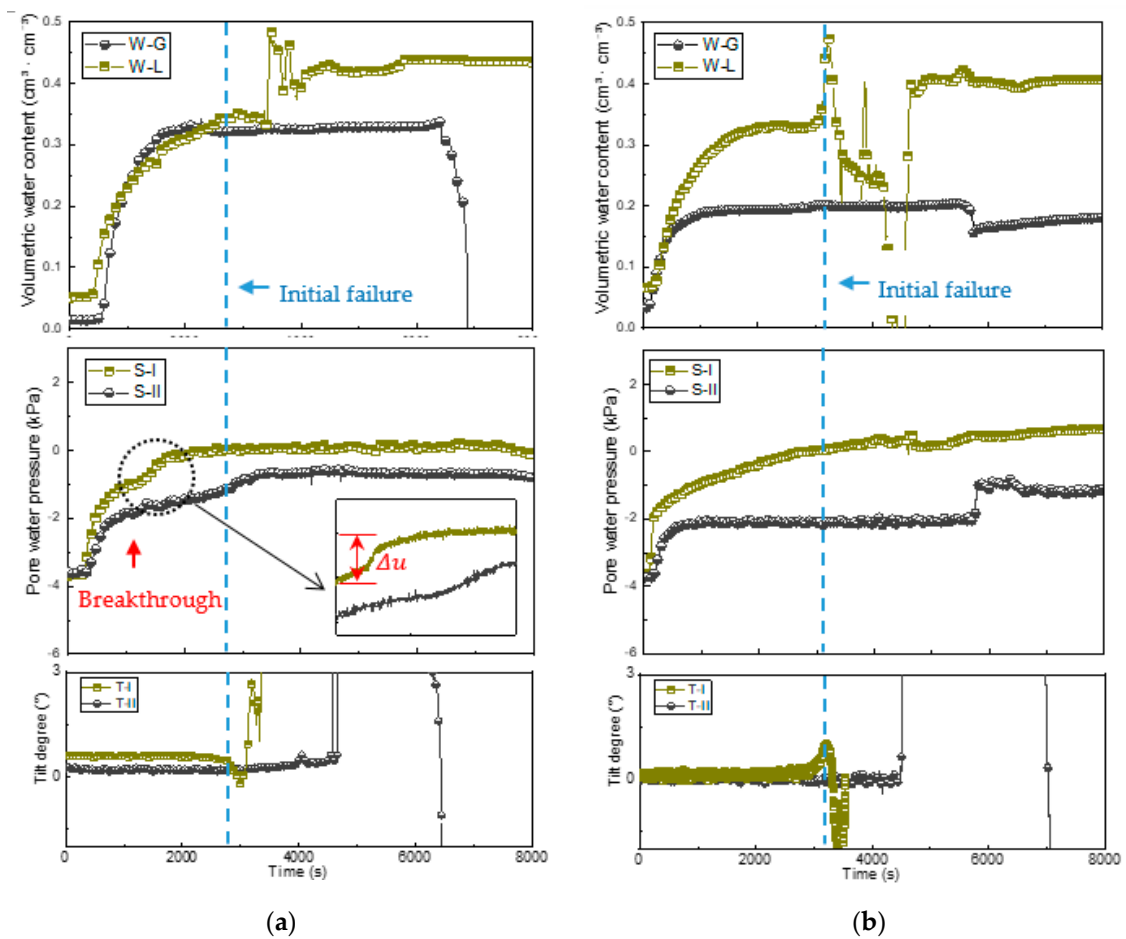


**Figure 11.** Volumetric water content, pore water pressure, and tilt angle change trends at different locations during infiltration. (a) Case III (tilt angle  $\alpha = 15^\circ$ , multi-layer), where the pore water pressure increased after capillary barrier breakthrough; (b) case VII (tilt angle  $\alpha = 15^\circ$ , single layer). For the positions of sensors, see Figure 3b.

### 3.2.5. Capillary Barrier Restoration in the Drying Process ( $t = 3.5\text{--}36\text{ h}$ )

The VWC in soil decreased once the rainfall stopped in case I (Figure 9a) and V ((Figure 9c). However, the bottom of the upper fine layer maintained a higher water content condition at 0.33 compared with the single-layer slope, which was only 0.19 in case I and V, respectively. The capillary barrier broken through could be restored to its pre-breakthrough condition once rainfall had stopped. The VWC of the finer soil above the interface decreased as the rainfall water continued to drain out. As the VWC at the interface decreased, the unsaturated hydraulic conductivity of the coarser lower layer also decreased, and eventually approached zero. The capillary barrier was completely restored when the intermediate coarser layer could not accept any more rainfall water from the overlying fine layer.

## 3.3. Influence of the Tilt Angle

### 3.3.1. Influence of the Tilt Angle on Water Movement

To show the water movement and its lateral diversion length in a multi-layer slope, the slope surfaces were marked with blue colors before the rainfall. With the aid of the backlighting and the dye traces, it was simple to visualize the dyed streamlines with the water movement once a steady state was achieved. The lateral diversion length and breakthrough zone could also be measured directly. Figure 11 shows photographs of the dyed trace streamlines from single-layer and multi-layer



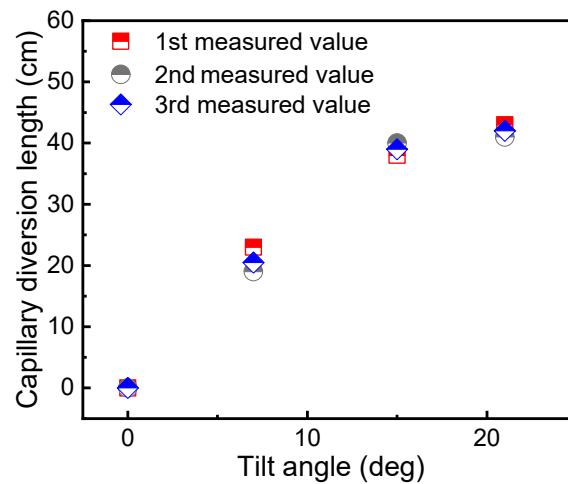


**Figure 13.** Effect of the tile angle on the capillary barrier diversion length in a multi-layer slope in case I, II, III, and IV (each case was performed three times for the same experimental conditions).

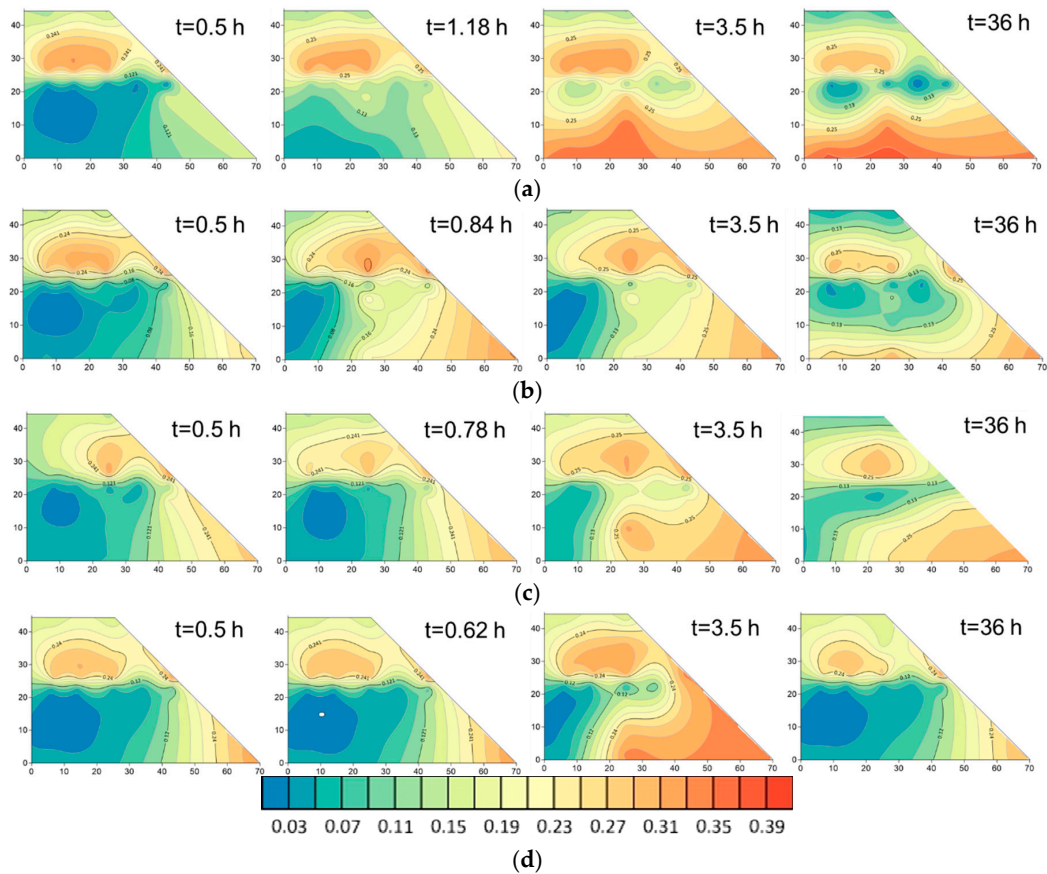


**Figure 14.** The VWC changes with elapsed time in case I, II, III, and IV (the VWC distribution after slope failure was verified by obtaining soil samples from various locations at the end of the test). (a) Case I. Multi-layer slope, 0 deg, 75 mm/h; (b) Case II. Multi-layer slope, 7 deg, 75 mm/h; (c) Case III. Multi-layer slope, 15 deg, 75 mm/h; (d) Case VII. Multi-layer slope, 21 deg, 75 mm/h.

### 3.3.2. Influence of the Tilt Angle on the Pore Pressure and VWC

To investigate the effects of the tilt angle, the pore pressure sensor (S-I) and VWC sensor (W-L) at the bottom were considered for comparison in different cases, as these are most crucial to the

knowledge on slope failure. Detailed in Figure 14 is the progressive build-up of VWC and pore water pressure throughout the experiments I, III, and IV, until failure occurred.

For Figure 15a,b, it is clear that an increased tilt angle has a drastic effect on the build-up of volumetric water content and pore water at the bottom of the slope, progressively resulting in quicker failure times as the tilt angle increases.

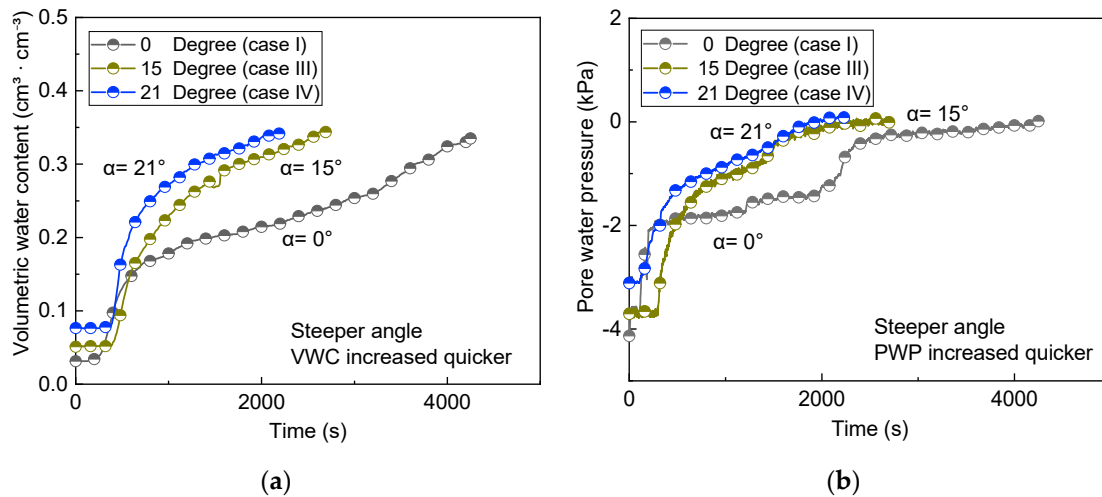


**Figure 15.** Time series of the VWC and pore pressure at the bottom of the slope for case I, III, and IV, with  $\alpha$  ranging from  $0^\circ$  to  $21^\circ$  (multi-layer slope). (a) Time series of the VWC from initiation to failure; (b) time series of the pore pressure from initiation to failure.

Once the wetting front arrived, sensor spikes in measurements occurred. It took around 1.18, 0.78, and 0.62 h for the pressure head and VWC to approach the maximum value in case I, III, and IV, respectively. The peak value of VWC and pore pressure values were similar for each case ranging between 0.348 and 0.351 and  $-0.021$  and  $-0.016$  kPa, respectively, at times of failure. Due to the rapid progression of the wetting front at an increased tilt angle, the pore water pressure and VWC increased at a faster rate, as is evident in results showing that the  $\alpha = 21^\circ$  (case V) failed 47% sooner than  $\alpha = 0^\circ$  (case I) and 34% sooner than  $\alpha = 15^\circ$  (case III). These similar trends were exhibited in all experiments where the tilt angle was increased [27].

## 4. Discussion

### 4.1. Mechanism of the Capillary Barrier

A capillary barrier (Figure 16a) forms in unsaturated conditions when the hydraulic conductivity of finer soil is higher than that of coarse soil, which limits the downward infiltration of water due to the difference of the hydraulic conductivity. Figure 15b shows the relations between the hydraulic conductivity and suction of the two sands measured in the lab. The intersect of two hydraulic conductivity curves is 0.4 kPa. From the intersect to the higher suction (suction  $> 0.4$  kPa), the hydraulic conductivity in the coarse layer is much lower than that in the fine layer, which caused the capillary barrier to form at the fine-coarse interface. Otherwise, suction at the interface decreased gradually after the wetting front arrived and was located to the left of the intersection, and the hydraulic conductivity in the coarse layer was higher than that of the fine one, which allowed the rainfall water to infiltrate into the next layer after capillary barrier breakthrough.

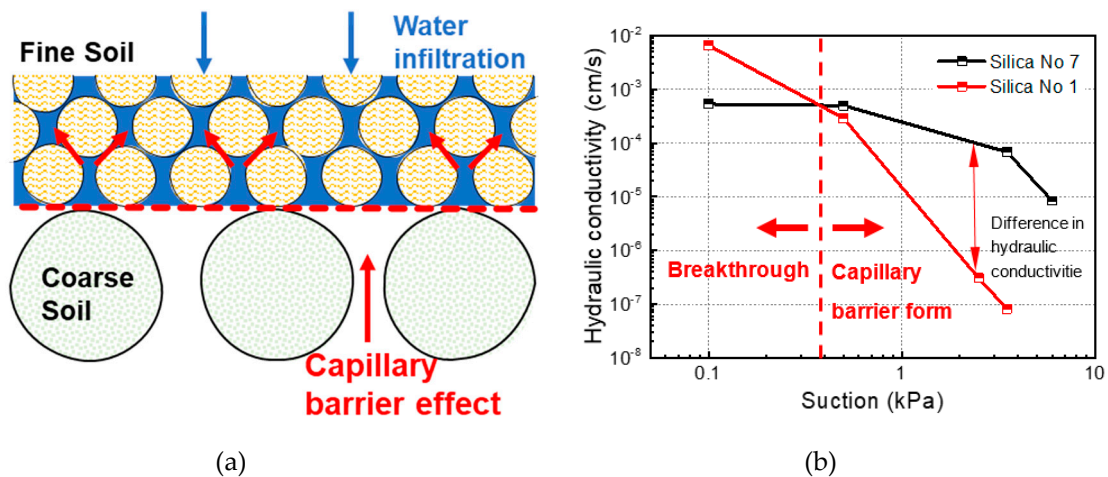


**Figure 16.** (a) Capillary barrier at the interface between different layers with different conductivities. (b) The relationship between the hydraulic conductivity and suction of silica No 1 and No 7.

4.2. D Flow and Multi-Layer Slope Stability

As is shown in Figure 17a, the blue color was used to stain the surface of the slope and to show the movement of rainfall water, and it was applied under the coarse layer to check that the capillary barrier still worked. At the beginning of case III, the water flow showed a vertical movement, mainly controlled by gravity, before the wetting front arrived at the interface. Secondly, the water flow could not go across the interface directly upward of the slope and showed a significant velocity component parallel to the inclined interface after the wetting front arrived [28].

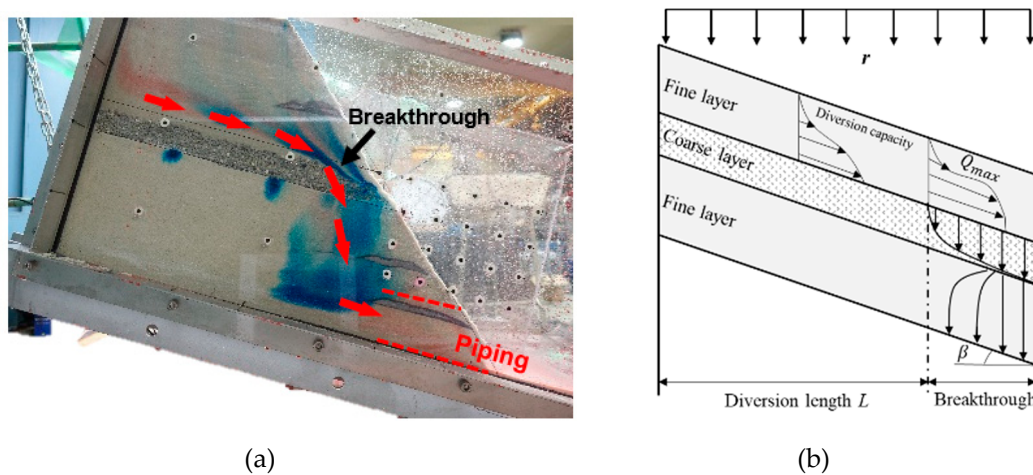


**Figure 17.** (a) Side view of the diversion length and breakthrough area of the capillary barrier (the movement and the breakthrough zone are shown by the blue dye traces); (b) calculation of the capillary diversion length  $L$ .

Lateral diversion is essentially gravity-driven unsaturated drainage within the finer layer of a sloped capillary barrier [29,30]. The unsaturated hydraulic conductivity is the maximum as the VWC of the upper finer soil increases with depth, where lateral diversion is concentrated at the fine-coarse interface. Besides, the diverting water will increase the water content in the downslope direction with the influence of the inclined angle, which may result in failure of the barrier and then infiltrate into the next layer.

In Figure 17b, the maximum length of the capillary diversion can be calculated by [31]:

$$K(\psi) = \frac{\{1-(\alpha\psi)^{mn}[1+(\alpha\psi)^n]^{-m}\}^2}{[1+(\alpha\psi)^n]^{m/2}} * K_s \quad (2)$$

$$L \leq \tan(\beta) \frac{K(\psi)}{q} \left[ \frac{1}{\alpha} + (|\psi_a| - |\psi_w^*|) \right] \quad (3)$$

where,  $\psi$  is the matric suction in the soil;  $\psi_w^*$  is the water entry value of the coarse layer;  $\psi_a$  is the air entry value of the fine layer;  $\beta$  is the tilt angle of the slope ( $^\circ$ );  $r$  is the infiltration rate (mm/h);  $K(\psi)$  is the hydraulic conductivity of the fine layer; and  $a$ ,  $m$ , and  $n$  are the fitting parameters.

Physical model experiments with a tilt angle  $\alpha = 0^\circ, 7^\circ, 15^\circ$ , and  $21^\circ$  were performed three times in order to ensure the repeatability of the results. An important point to be noted is that every physical model was assumed to be identical, but there were slight differences in the model construction and preparation process, which could have resulted in some dissimilarity between experiments. Taking this fact into account, the result of the capillary diversion length at different tilt angles (Figure 18a), which produced similar results, demonstrated the repeatability of the experiment. The pictures of failure situations in case III (tilt angle  $\alpha = 7^\circ$ ) are described in detail in Figure 18b. Although the details of soil piping of each experiment were unique, the results of different experiments were consistent.

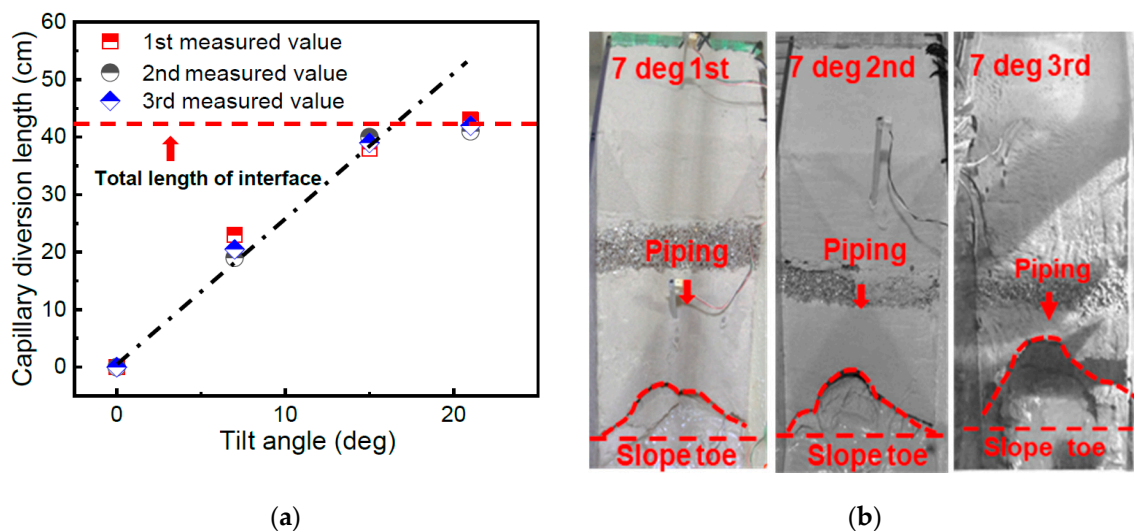


**Figure 18.** (a) Repeatability of the capillary diversion length (tilt angle  $\alpha = 0^\circ, 7^\circ, 15^\circ$ , and  $21^\circ$ , where each case was performed three times to ensure the repeatability of the results); (b) experiments of failure situations were conducted in case III under the same experimental conditions three times.

The capillary barrier effects caused by the inter-mediate coarser layer initially confines the rainwater infiltration in the uppermost soil. Depending on the characteristics of rainfall and the inclined angle condition, top finer soils are almost permanently unsaturated [32]. In some slope steeper than  $40^\circ$  at higher elevations, this may lead to instability of the top fine soil before capillary barrier breakthrough, when the coarse layer and bottom layer are still far from the point of saturation [33]. Depending on the slope angle and shear strength of soil, failure can occur at the bottom before complete saturation, while the pore water pressure is still negative. These phenomenon in natural slope seem to disprove the possibility of failure mechanism due to piping in this study.

In our experiment, the piping failure occurred above the impermeable layer after the loss of the capillary barrier. This is consistent with the field investigation of the development of soil pipe in the base of the fine soil [34]. However, the actual mechanism of soil piping in these slope that still remains unclear. Some mechanisms have been proposed by previous researches to explain this

phenomenon such as internal erosion, flowslides and grain coarsening [34,35]. Internal erosion of the finer soil fraction driven by the seepage forces is thought to have played a significant influence on the slope failure [36,37]. It seems reasonable that the rainfall water caused the build-up of excess pore water pressure inside slope and the water inflow occurred during the rainfall condition, as the sharp increase of pore water pressure  $\Delta u$  measured at base of multi-layered slope (see Figure 10a). Further measurement such as the pore water pressure inside slope, internal displacements are still needed to improve the understanding of mechanism of failure of the slope [38].

## 5. Conclusions

Four groups of laboratory model experiments were performed to investigate the water movement, failure time, and modes in multi-layer and single-layer slopes caused by rainfall infiltration. In addition, the unsaturated hydraulic conductivity and SWCCs were also measured in the lab to clarify how the capillary barrier works under different conditions.

The results of hydraulic conductivity show that the unsaturated hydraulic conductivity  $K$  in the coarse layer is lower than that in the fine layer in a lower suction condition (0.4 kPa), which results in the development of the capillary barrier at the interface of the fine-coarse layer.

Different failure modes occurred in an inclined multi-layer slope and single-layer slope: sliding and piping failure. In the flat group, the capillary barrier was presented, which prevented the rainwater from infiltrating into the coarse layer for a while and caused a delay of the failure time. However, in the inclined group, the inclined intermediate coarser layer formed a capillary barrier, resulting in a significant amount of water being diverted to the downward slope and causing piping failure at the toe of the slope that resulted in earlier failure, which has a negative influence on the slope stability.

An increased tilt angle has a drastic effect on the capillary diversion length, in which more infiltrate water will be diverted to the downslope side and then infiltrate into the bottom of slope, resulting in quicker failure times.

The present study does not provide a model to be used in a specific site problem. Instead, the model is suitable for studies on hypothetical multi-layer hillsides to assess water movement patterns and general failure mechanisms. The results from such studies can prove useful in the development of an appropriate strategy for resolving problems in individual, site-specific multi-layer slopes.

In the present manuscript, we have mainly focused on the influence of the tilt angle and the effect of the capillary barrier on water movement and slope failure modes compared with a single-layer slope. It should be noted that in multi-layer slopes, different geometric characteristics, such as different heights, slope ratios, and fronts, also have an influence on the water infiltration and water content distribution in the slopes, significantly affecting slope failure initiation. Model experiments with different geometries of the shallow soil cover will be conducted in further research [39].

**Author Contributions:** Conceptualization, J.T. and U.T.; investigation, D.H.; methodology, S.T.; resources, J.X.; supervision, U.T.; Writing—original draft, J.T. All authors have read and agreed to the published version of the manuscript.

**Funding:** This research was supported by a Japanese Government Scholarship for PhD studies of the first author, the Sichuan Science and Technology Program (2018JY0613), Grants-in-Aid for Scientific Research of Japan Society for the Promotion of Science (JSPS), and Research Fellowships of Japan Society for the Promotion of Science for Young Scientists.

**Acknowledgments:** The authors would like to thank the reviewers for constructive comments that improved the paper.

**Conflicts of Interest:** The authors declare no conflict of interest.

## References

1. Santi, P.M. Debris-flow hazards and related phenomena: (Edited by matthias jakob and oldrich hungri). *Environ. Eng. Geosci.* **2007**, *13*, 75. [[CrossRef](#)]

2. Sidle, R.C.; Ochiai, H. Landslides: Processes, prediction, and land use. In *Water Resources Monograph*; American Geophysical Union: Washington, DC, USA, 2006.
3. Mancarella, D.; Simeone, V. Capillary barrier effects in unsaturated layered soils, with special reference to the pyroclastic veneer of the Pizzo d'Alvano, Campania, Italy. *Bull. Eng. Geol. Environ.* **2012**, *71*, 791–801. [[CrossRef](#)]
4. Webb, R.W.; Fassnacht, S.R.; Gooseff, M.N.; Webb, S.W. The presence of hydraulic barriers in layered snowpacks: TOUGH2 simulations and estimated diversion lengths. *Transp. Porous Media* **2018**, *123*, 457–476. [[CrossRef](#)]
5. Khire, M.V.; Benson, C.H.; Bosscher, P.J. Capillary Barriers: Design Variables and Water Balance. *J. Geotech. Geoenviron. Eng.* **2000**, *126*, 695–708. [[CrossRef](#)]
6. Abdolahzadeh, A.M.; Vachon, B.L.; Cabral, A.R. Evaluation of the effectiveness of a cover with capillary barrier effect to control percolation into a waste disposal facility. *Can. Geotech. J.* **2011**, *48*, 996–1009. [[CrossRef](#)]
7. Rahardjo, H.; Santoso, V.A.; Leong, E.C.; Ng, Y.S.; Tam, C.P.H.; Satyanaga, A. Use of recycled crushed concrete and Secudrain in capillary barriers for slope stabilization. *Can. Geotech. J.* **2013**, *50*, 662–673. [[CrossRef](#)]
8. Garcia, E.F.; Gallage, C.P.K.; Uchimura, T. Function of permeable geosynthetics in unsaturated embankments subjected to rainfall infiltration. *Geosynth. Int.* **2007**, *14*, 89–99. [[CrossRef](#)]
9. Morel-Seytoux, H.J.; Nimmo, J.R. Soil water retention and maximum capillary drive from saturation to oven dryness. *Water Resour. Res.* **1999**, *35*, 2031–2041. [[CrossRef](#)]
10. Kämpf, M.; Holfelder, T.; Montenegro, H. Identification and parameterization of flow processes in artificial capillary barriers. *Water Resour. Res.* **2003**, *39*, 1–9. [[CrossRef](#)]
11. Rulon, J.J.; Freeze, R.A. Multiple seepage faces on layered slopes and their implications for slope-stability analysis. *Can. Geotech. J.* **1985**, *22*, 347–356. [[CrossRef](#)]
12. Hideki, I. Relationship between slope failure and the active fault based on kumamoto earthquake in 2016 and following heavy rainfall induced disaster. *J. Jpn. Soc. Eng. Geol.* **2017**, *58*, 188–196.
13. Matsushi, Y.; Hattanji, T.; Matsukura, Y. Mechanisms of shallow landslides on soil-mantled hillslopes with permeable and impermeable bedrocks in the Boso Peninsula, Japan. *Geomorphology* **2006**, *76*, 92–108. [[CrossRef](#)]
14. Hamrouni, F.; Trabelsi, H.; Jamei, M.; Olivella, S. Numerical analysis of landslides caused by rainfall in a reduced physical slope model. *Eur. J. Environ. Civ. Eng.* **2019**, *0*, 1–22. [[CrossRef](#)]
15. Hillel, D. *Environmental Soil Physics: Fundamentals, Applications, and Environmental Considerations*; Elsevier: Amsterdam, The Netherlands, 1998; ISBN 0080544150.
16. Wang, C.; Mao, X.; Hatano, R. Modeling ponded infiltration in fine textured soils with coarse interlayer. *Soil Sci. Soc. Am. J.* **2014**, *78*, 745–753. [[CrossRef](#)]
17. Yang, H.; Rahardjo, H.; Leong, E.C.; Fredlund, D.G. A study of infiltration on three sand capillary barriers. *Can. Geotech. J.* **2004**, *41*, 629–643. [[CrossRef](#)]
18. Mancarella, D.; Doglioni, A.; Simeone, V. On capillary barrier effects and debris slide triggering in unsaturated layered covers. *Eng. Geol.* **2012**, *147–148*, 14–27. [[CrossRef](#)]
19. Damiano, E.; Greco, R.; Guida, A.; Olivares, L.; Picarelli, L. Investigation on rainwater infiltration into layered shallow covers in pyroclastic soils and its effect on slope stability. *Eng. Geol.* **2017**, *220*, 208–218. [[CrossRef](#)]
20. Hillel, D. *Introduction to Soil Physics*; Academic Press: Cambridge, MA, USA, 1982.
21. Van Genuchten, M.T. A closed-form equation for predicting the hydraulic conductivity of unsaturated soils. *Soil Sci. Soc. Am. J.* **1980**, *44*, 892–898. [[CrossRef](#)]
22. Evett, S.R.; Tolk, J.A.; Howell, T.A. Soil profile water content determination: Sensor accuracy, axial response, calibration, temperature dependence, and precision. *Vadose Zone J.* **2006**, *5*, 894–907. [[CrossRef](#)]
23. Di Matteo, L.; Pauselli, C.; Valigi, D.; Ercoli, M.; Rossi, M.; Guerra, G.; Cambi, C.; Ricco, R.; Vinti, G. Reliability of water content estimation by profile probe and its effect on slope stability. *Landslides* **2018**, *15*, 173–180. [[CrossRef](#)]
24. Zhan, L.T.; Li, G.Y.; Jiao, W.G.; Wu, T.; Lan, J.W.; Chen, Y.M. Field measurements of water storage capacity in a loess-gravel capillary barrier cover using rainfall simulation tests. *Can. Geotech. J.* **2017**, *54*, 1523–1536. [[CrossRef](#)]
25. Sinai, G.; Zaslavsky, D.; Golany, P. The effect of soil surface curvature on moisture and yield—Beer sheba observation. *Soil Sci.* **1981**, *132*, 367–375. [[CrossRef](#)]

26. Yeh, W.W.-G. Reservoir Management and operations models: A state-of-the-art review. *Water Resour. Res.* **1985**, *21*, 1797–1818. [[CrossRef](#)]
27. Xie, J.; Uchimura, T.; Chen, P.; Liu, J.; Xie, C.; Shen, Q. A relationship between displacement and tilting angle of the slope surface in shallow landslides. *Landslides* **2019**, *16*, 1243–1251. [[CrossRef](#)]
28. Junfeng, T.; Taro, U.; Shangning, T.; Dong, H.; Jiren, X. Water movement and deformation in unsaturated multi-layered slope under heavy rainfall. *Int. J. Geomate* **2020**, *19*, 174–181. [[CrossRef](#)]
29. Morris, C.E.; John, C. Stormont parametric study of unsaturated drainage layers in a capillary barrier. *J. Geotech. Geoenviron. Eng.* **1999**, *125*, 1057–1065.
30. Morris, C.E.; Stormont, J.C. Capillary barriers and subtitle D covers: Estimating equivalency. *J. Environ. Eng.* **1997**, *123*, 3–10. [[CrossRef](#)]
31. Walter, M.T.; Kim, J.S.; Steenhuis, T.S.; Parlange, J.Y.; Heilig, A.; Braddock, R.D.; Selker, J.S.; Boll, J. Funneled flow mechanisms in a sloping layered soil: Laboratory investigation. *Water Resour. Res.* **2000**, *36*, 841–849. [[CrossRef](#)]
32. Calcaterra, D.; Parise, M.; Palma, B.; Pelella, L. The influence of meteoric events in triggering shallow landslides in pyroclastic deposits of Campania, Italy. *Hazards Mitig.* **2000**, *11*, 99–107.
33. Del Prete, M.; Guadagno, F.M.; Hawkins, A.B. Preliminary report on the landslides of 5 May 1998, Campania, southern Italy. *Bull. Eng. Geol. Environ.* **1998**, *57*, 113–129. [[CrossRef](#)]
34. Hu, W.; Dong, X.J.; Xu, Q.; Wang, G.H.; van Asch, T.W.J.; Hicher, P.Y. Initiation processes for run-off generated debris flows in the Wenchuan earthquake area of China. *Geomorphology* **2016**, *253*, 468–477. [[CrossRef](#)]
35. Wang, G.; Sassa, K. Factors affecting rainfall-induced flowslides in laboratory flume tests. *Géotechnique* **2001**, *51*, 587–599. [[CrossRef](#)]
36. Hu, W.; Scaringi, G.; Xu, Q.; Huang, R. Internal erosion controls failure and runout of loose granular deposits: Evidence from flume tests and implications for postseismic slope healing. *Geophys. Res. Lett.* **2018**, *45*, 5518–5527. [[CrossRef](#)]
37. Hu, W.; Scaringi, G.; Xu, Q.; Pei, Z.; Van Asch, T.W.J.; Hicher, P.Y. Sensitivity of the initiation and runout of flowslides in loose granular deposits to the content of small particles: An insight from flume tests. *Eng. Geol.* **2017**, *231*, 34–44. [[CrossRef](#)]
38. Huang, A.B.; Lee, J.T.; Ho, Y.T.; Chiu, Y.F.; Cheng, S.Y. Stability monitoring of rainfall-induced deep landslides through pore pressure profile measurements. *Soils Found.* **2012**, *52*, 737–747. [[CrossRef](#)]
39. Tao, S.; Uchimura, T.; Fukuhara, M.; Tang, J.; Chen, Y.; Huang, D. Evaluation of soil moisture and shear deformation based on compression wave velocities in a shallow slope surface layer. *Sensors* **2019**, *19*, 3406. [[CrossRef](#)]

